Next Materials 9 (2025) 101149

Contents lists available at ScienceDirect

Next Materials

journal homepage: www.sciencedirect.com/journal/next-materials

Research article

Processing and EPR characterization of europium, thulium co-doped yttria (YET) powders for radiation dosimetry

S.C. Santos *, Jr O. Rodrigues, L.V. E. Caldas

Instituto de Pesquisas Energeticas e Nucleares – IPEN, Av. Prof. Lineu Prestes 2242, Cidade Universitaria, Sao Paulo, Brazil

ARTICLE INFO

Keywords:
Europium
Thulium
Yttria
Rare-earths
EPR
Radiation dosimetry

ABSTRACT

Radiation dosimetry demands a continuous effort in development of new materials due to its essential purpose, accuracy and quality assurance in all procedures in which radiation energy is used. Rare-earths are critical materials due to their great chemical and physical properties, whose applicability has been shown very relevant in radiation dosimetry. The present study reports an approach to obtain europium, thulium co-doped yttria powders (YET) by an alternative hydrothermal synthesis for application in radiation dosimetry. According to results, the proposed synthesis method provided YET powders with cubic C-type form, flake-like shape, and narrow particle-size distribution with mean diameter (d_{50}) of 148 nm. Moreover, the EPR spectra of the as-synthesized powders exhibited a resonance peak recorded at 335.52mT, with g-value of 2.0094, and peak-width of 3.23mT. As exposed to ionizing radiation (^{60}Co) in a range of dose from 1 to 20 kGy, YET powders exhibited distinct dose-response behaviour as a function of dose, including a slight change in g-factor. These findings are substantial parameters to go forward in formation of new materials for radiation dosimetry.

1. Introduction

Radiation dosimetry [1] field has the aim to guarantee precision and reproducibility in measurement of dose in practices in which ionizing radiation is used as food [2], agriculture [3], clinical [4], and industry [5]. Thus, it demands a progressive and effective effort of materials development, where it is expected of these new materials the capability of providing great sensitivity and dose-response behaviour. Besides, the formulation of materials composition and synthesis are essential strategies to succeed in this purpose.

Rare-earth (RE) based materials are considered critical materials [6–9] due to their unique chemical and physical properties, and have shown great applicability in radiation dosimetry. Gedam et al. [10] observed that the thermoluminescence (TL) response of $NaZnSO_4Cl$ phosphors was improved by doping it with Ce. Nagabhushana et al. [11] reported that the incorporation of Pr^{3+} ions introduced deeper traps and significantly enhanced the thermal stability and TL response of Ca_2SiO_4 phosphors. Kadam et al. [12] found out Y, Eu co-doped $LiCaAlF_6$ exhibits great Optically Stimulated Luminescence (OSL) sensitivity, where the minimum detectable dose (MDD) could be achieved in the range of 0.1–0.2μGy. Moreover, yttria (Y_2O_3), whose synonym is yttrium oxide, has been successfully used as host material of other rare-earth (RE) metals due to its lattice characteristics [13], and physical-chemistry similarity with RE. As a result, RE-doped yttria has shown improved characteristics as luminescence [14], electrical conductivity [15], chemical strength [16], thermal shock [17], and paramagnetic response [18].

Powder synthesis [19] has the aim to form particles with controlled characteristics as, size distribution [20], surface area [21], and shape [22]. Besides, particle characteristics play an important role during processing such as mixing [23], dispersion [24], shaping [25], and sintering [26]. Moreover, the microstructure formation and materials applicability [27] relies on particle characteristics. Recent studies of the group have shown the advantage of using a low temperature hydrothermal synthesis for producing nanoparticles with controlled size and shape as, β-yttrium disilicate (β-$Y_2Si_2O_7$) [28], dysprosium doped yttrium disilicate ($Y_2Si_2O_7$:Dy) [29], and europium doped yttria (Y_2O_3:Eu) [30], and thulium doped yttria (Y_2O_3:Tm) [31].

While previous studies of the group [32] concerned with synthesis and conventional characterization of the YET particles, the present one reports a step forward in the search of new postulating materials for radiation dosimetry. This work innovates by reporting an EPR study on the formation of radiation induced radicals in the YET particles as exposed to ionizing radiation (^{60}Co source) in a range of dose from l to

* Corresponding author.
E-mail address: silas.cardoso@alumni.usp.br (S.C. Santos).

https://doi.org/10.1016/j.nxmate.2025.101149
Received 15 May 2025; Received in revised form 31 July 2025; Accepted 27 August 2025
Available online 30 August 2025

20 kGy. Particle characteristics as size distribution, shape, and crystalline form are evaluated. Besides, the effect of ionizing radiation on paramagnetic radicals in YET particles is discussed. These achievements are essential to advance toward the formation of new materials based on rare-earth oxides for radiation dosimetry.

2. Experimental

Europium, thulium co-doped yttria powders (YET) were formed by hydrothermal synthesis as described in our previous study [30]. The acronym YET comes from Y as yttria (Y_2O_3), E as europium oxide (Eu_2O_3), and T as thulium oxide (Tm_2O_3), while the composition of the YET powders is 2 at%E, 1 at%T (at%, atomic percentage), considering the best results achieved in ours previous study [32].

The crystalline structure of the YET powders was evaluated by X-ray diffraction (XRD, Rigaku Multiflex), at room temperature, angular range (2θ) 25–80°, step size of 0.5°.min^{-1}, and CuK$\alpha_{1,2}$ radiation source. The identification of the crystalline structure and indexing of lattice planes (h, k, l) were performed by Rietveld refinement using Profex [33] software. Electron density maps were obtained from the refinement data of the observed structures. A graphical representation of the crystal lattice was built up by Vesta [34] software. Furthermore, a phase diagram of rare-earth sesquioxides [35] was used to predict and support the crystallography findings.

Particle size distribution (d_{10}-d_{90}) of the YET powders was determined by Photon Correlation Spectroscopy [36] (PCS, Litesizer500, Anton Paar), while their morphology were observed by using a Scanning Electron Microscope (SEM, Inca-X, Oxford Instruments).

YET powders were exposed to ionizing radiation source (^{60}Co) under environmental atmosphere and temperature, in a range of dose from 1 up to 20 kGy in electronic equilibrium. Afterwards, their paramagnetic response as a function of dose were evaluated by electron paramagnetic resonance spectroscopy (EPR), using an X-band magnetic spectrometer (Bruker EMX PLUS). The EPR spectra were recorded at 20 °C, room atmosphere, 10 scans, modulation amplitude of 4 G, sweep time of 10.02 s, field modulation frequency of 100 kHz, microwave power of 2.5 mW, center field of 300mT, sweep width of 300mT, time constant of 0.01 ms, controlled humidity, and a DPPH (2, 2-Diphenyl-1-picrylhydrazyl, Bruker) as reference. All EPR spectra were evaluated considering their features as peak-to-peak amplitude (ppa), peak-to-peak width (pw), and g-value. Three powered samples (81.98 mg) were used for each EPR measurement, and an average spectra was obtained for evaluation. The normalisation of the EPR measurements was performed by dividing the average EPR spectra intensity by sample mass, followed by peak-to-peak amplitude of the DPPH standard (1,1-Difenil-2-Picril-Hidrazil).

3. Results and discussion

The Rietveld refinement of YET powdered composition is illustrated in Fig. 1a. The observed spectra (salmon solid line) is mostly attributed to cubic C-type form of yttria, which exhibits four high intensity diffraction peaks recorded at 29.5°, 34.5°, 48.5°, and 58.5°, respectively. Besides, two additional low intensity diffraction peaks at 31.5° and 33.5° related to θ-Al_2O_3 (BGMN file 01–086–1410) were observed. This result is associated to the presence of 4.3ppb Al (parts per billion) in the composition of the starting materials (appendix A). Szanyi et al. [37] r reported a great review on alumina polymorphs derived from boehmite [38], where is stated that θ-Al_2O_3 is achieved at temperatures of ~950–1000°C.

The refinement/calculated spectra (darkorchid circles) fits the observed pattern (salmon solid line), where the difference between the observed spectra (salmon line) and the calculated (darkorchid circles) is illustrated by the green curve (Fig. 1b). Besides, the brown solid lines (Fig. 1c) represent yttria indexed planes (h, k, l) according to the BGMN reference (04–005–4378), while the darkblue solid lines (Fig. 1d) represent θ-Al_2O_3 indexed planes based on the BGMN reference (01–086–1410). The main Rietveld refinement results were R of 8.87 %, R_w of 12.35 %, R_{exp} of 8.45 %, χ^2 of 2.1361, G_of of 1.4615, crystallite size (d_c) of 35.5 ± 1.1 nm, and crystal density (ρ_{XRD}) of 5.031 g.cm^{-3}.

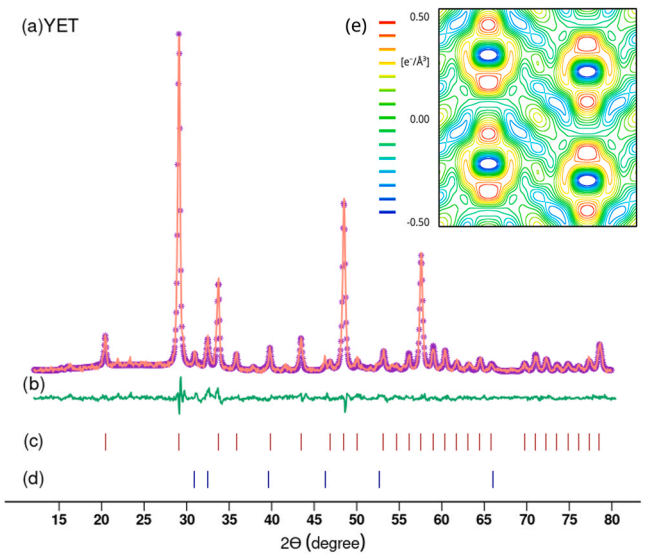

Fig. 1. Rietveld refinement of YET powders: (a) salmon solid line is the experimental data, darkorchid circles are the calculated pattern; (b) mediumseagreen solid line is the residual pattern (experimental – calculated); (c) brown solid lines are the indexed peaks of Y_2O_3, while those (d) darkblue are attributed to θ-Al_2O_3; (e) electron electron density map.

The Rietveld method also provides a significant data to illustrate the distribution of electrons into a unit cell, and this graphical representation is known as electron density map (Fig. 1d). Red contours indicate the electron distribution of yttrium (Y) atoms, whereas light blue lines contours indicate those from oxygen (O) atoms. The enhancement of red lines is attributed to the presence of the rare-earth dopants as europium (Eu), and thulium (Tm). Additionally, it is evidenced that yttria lattice exhibits many oxygen vacancies represented as green lines contours and due to this feature yttria is used as a host material for dopping with other rare-earth ions. The insertion of another rare-earth ion lead to to improve yttria characteristics such as thermal-erosion resistence [39], sinterability [40], optical properties [41], electrical conductivity [42], and dosimetric materials [43]. Studies performed by our group on colloidal processing of yttria based ceramics have shown the potential of yttria for radiation dosimetry. Europium-yttria (YE) rods exhibited a significant and linear EPR dose-response behaviour in a range of dose from 0.01 to 10 kGy[44]. While, thulium-yttria (YTm) powders presented more effective response to dose than those of “pure” yttria [45]. Recently, it was reported [46] that YTm rods sintered at 1600°C for 2 h exhibited linear dose-response behaviour in a range of dose from 0.001 to 1 kGy.

The XRD result illustrated in Fig. 1 reveals that the doping process of yttria using Tm^{3+} and Eu^{3+} ions was effective. Upon crystal lattice, the ionic radius of Eu, Tm and Y are relatively similar 0.098, 0.109, and 0.092 nm, respectively, and therefore the character of doping is substitutional. Thus, Eu and Tm ions replace Y ions at C_2 and S_6 sites with no significant distortion of crystal lattice. It is expected that doping with europium and thulium can give rise of a great number of electron defects in yttria lattice and enhance its electronic features for dosimetry applications. The beneficial effects of substitutional doping has been reported elsewhere [47–51].

Yttria in cubic C-type form exhibits 16 unit formula (YO_6), with 32 cations that constitutes 24 sites of C_2 symmetry, 8 sites of C_{3i} symmetry and space group C_2 and C_{3i},S_6 (Fig. 2a–c). As illustrated in Fig. 2d and highlighted in light blue dots, the C-type form is the most predominant

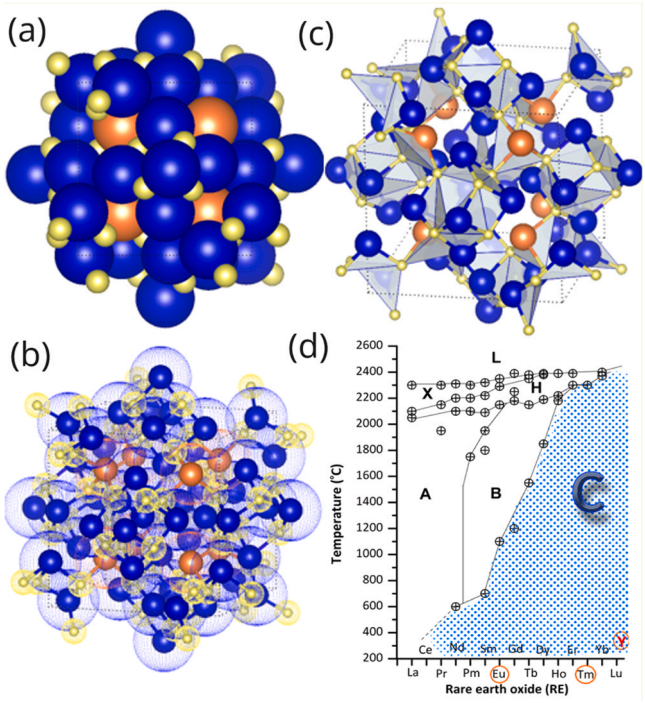

Fig. 2. Representation of the crystalline structure of yttria in cubic C-type form from XRD experimental data processed by Vesta software, where a unit cell is illustrated based on the style models (a) space-filling, (b) ball-and-stick with dot-surface, (c) polyhedral; and (d) phase diagram of rare-earth sesquioxides, where the cubic C-type form as the most predominant form is highlighted in blue dots.

crystalline structure for the majority of rare-earth (RE) based sesquioxides (RE_2O_3) [35]. Moreover, Y, Eu, and Tm based sesquioxides (highlighted in red) are stable in Cubic C-type up to the temperature limit of 2250°C, 1100°C, and 2200°C, respectively. The following forms A, B, H, and X are usually obtained by using both high pressure and high temperature [52–54]

Particle size distribution of YET powders by PCS is shown in Fig. 3a. According to results the powdered composition is constituted of a narrow particle distribution in nanosize range, characterized by a mean particle diameter (d_{50}) of 148 nm, span (S_p) of 69 nm, which is the difference between d_{90} and d_{50} fractions, and a relative span (R_s) of 0.5,

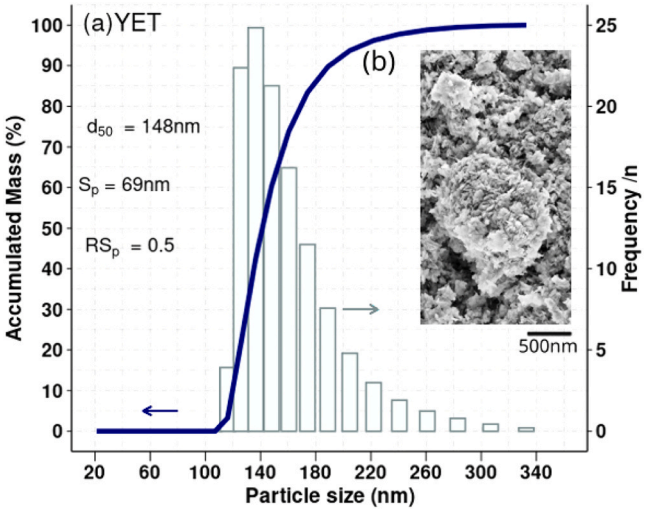

Fig. 3. (a) Particle size distribution by PCS; and (b) SEM image of flake-like particles.

which corresponds to the ratio between S_p and d_{50}.

Particles in nanosize range are useful in ceramic processing, seeing that they can form high-density powder compacts, which in turn, lead to development of advanced materials with controlled microstructure as sintered. Alves et al. [55] found out lithium disilicate samples prepared with glass-based powders (d_{50} of 1.7 μm) presented higher densification ($\rho \approx 96$ %) than those prepared with coarsed powders (d_{50} of 12 μm) and ($\rho \approx 92$ %). Moreover, nanoparticles usually promote the improvement of materials characteristics such as mechanical strength [56], electrical conductivity [57], hardness [58], corrosion resistance [59], luminescence [60], and radiation measurement [61]. The particle size distribution observed for YET powdered composition seems to be useful to prepare concentrated suspensions with the aim to form nanostructure materials for radiation dosimetry.

Based on the SEM image illustrated in Fig. 3b, it is observed that YET particles are constituted by agglomerate of flake-like particles, whose size is inferior than 200 nm. This result makes evident the synthesis method proposed was effective in producing ceramic particles in nano scale size. Like size, particle shape also can head the further steps of processing, such mixing [62], dispersion [63], shaping [64], and sintering [65]. Moreover, the particle shape has great influence on the formation and evolution of the material microstructure [66–71]. Considering the Dupont et al.[72] model to predict the formation and evolution of a ceramic powder compact, the YET flake-like powders tend to undergo the following densification stages: (1) motion of particles; (2) densification; and (3) grain growth.

The EPR spectra of YET nanoparticles as a function of dose is illustrated in Fig. 4. Based on results, it is clearly observed a main EPR peak (P_1) recorded at 335mT, which is attributed to interstitial oxygen ion from environmental atmosphere. In addition, this peak was considerably enhanced under irradiation of 10 kGy (gold line). A second peak (P_2) attributed to F^+ centre charged vacancy oxygen with one remaining electron, was observed at 343mT. On the other hand, the P_2 peak was not observed for samples exposed to irradiation up to 20 kGy, which indicates that occurred a full recombination of electron defects and paramagnetic radicals. The incorporation of Eu, and Tm ions into yttria lattice is performed by replacing Y^{3+} ions for Eu^{3+}/Tm^{3+} ions on yttria sites C_2 and C_{3i}. As discussed previously on XRD characterization (Fig. 1), there is a narrow difference between ions size (Y, Eu, and Tm) and the doping process is substitutional. Even if, no significant structural changes were observed, new electron defects, which includes vacancies

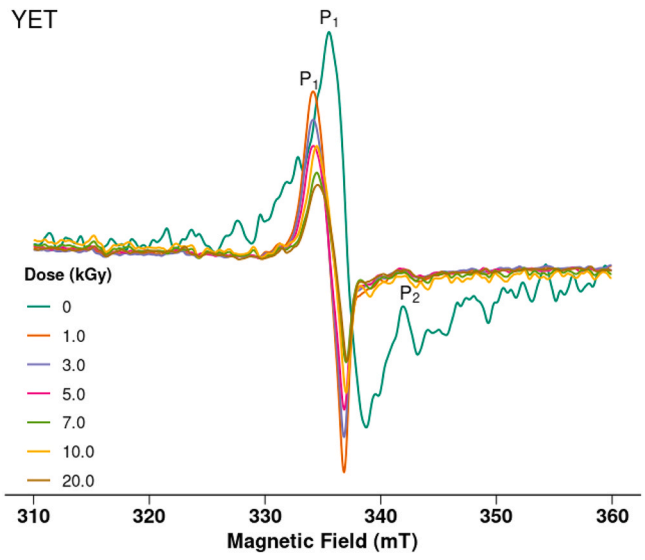

Fig. 4. Electron paramagnetic resonance spectra of the YET nanoparticles as a function of dose from 0 up to 20 kGy, and recorded under environmental atmosphere and temperature.

and unpaired electrons may be formed and during irradiation under 10 kGy these electron defects can be observed. During our investigation on europium doped yttria rods, four EPR peaks assigned to (a, b, c_1, and c_2) and recorded at 160, 249, 345 and 360mT were observed.

The g-value is a signature of an electron defect. As illustrated in Fig. 5, YET powders exposed to radiation doses ranging from 0 up to 20 kGy exhibited a slight variation of g-values from 2.0094 to 2.0177, and a span of 0.0083. As reported in literature [73–76], g-values around 2.0000 are usually assigned to oxygen vacancies $(V_{\ddot{O}})$. Osada et al.[77] achieved a g-value around 2.040 for Y_2O_3-CaO powdered samples, while Brown et al.[78] reported g-value of 2.0415 for Er:Y_2O_3 powders. The point defect $(V_{\ddot{O}})$is originally of yttria lattice, where Eu^{3+} and Tm^{3+} ions filled these empties sites. As a result, a small variation on g-values was recorded. However, $(V_{\ddot{O}})$can also be induced by processing conditions as thermal treatment (atmosphere, temperature, time, and electric field). Yttria oxygen vacancies enable the doping with rare-earth metals (RE), forming new materials (RE:Y_2O_3) with enhanced mechanical, chemical, and spectroscopic response. Moreover, oxygen vacancies drive the mechanism of flash joining as reported by Zhang et al.[79]

The EPR response of YET powders as a function of dose is illustrated in Fig. 6. Considering the peak-peak amplitude (PPA) of the main peak (P_1), it is clearly evidenced that no irradiated powders presented the highest EPR response around of 5.6.105a.u., while those exposed to ionizing radiation exhibited a decrement in PPA in a range of dose from 1 up to 20 kGy. This result makes evident the electron defects induced by doping with Eu and Tm ions under high dose irradiation recombine with each other, leading to decrement of EPR response. On the other words, Tm ions compete with Eu ions into yttria lattice, providing low concentration of electron defects. Additionally, Tm ions could have filled yttria sites that do not show a dosimetric response accordingly as exposed to high dose radiation. In a previous study performed by the group [80], it was achieved that doping yttria with 2 at%Eu led to improvement of EPR response in a range of dose from 1 up to 10 kGy. Even if the use of Tm and Eu was not effective in enhancing EPR response of yttria under high dose irradiation, the present result might be different using lower doses in a further investigation.

The effect of dose on peak-width (pw) of P1 peak is illustrated in Fig. 7. Based on the results, irradiation induced a narrowing effect on pw, ranging from 3.27mT (no dose) to 2.57 (20 kGy). The pw is due to the contribution from dipolar interaction between dopant and host spins, i.e in the present study Eu^{3+} and Tm^{3+} as dopants, and Y^{3+} as host. According to Mitsuma [81] the fast relaxation of host ions can randomly modulate the dipolar and exchange interaction between paramagnetic host and impurity ions, resulting in peak-width narrowing.

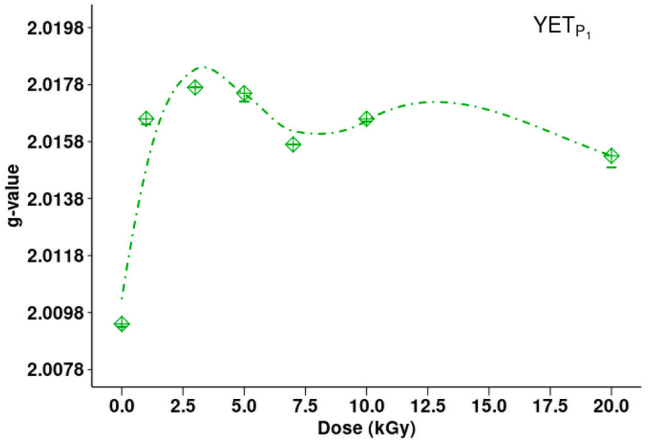

Fig. 5. Variation of the g-value of YET powders (peak P_1) as a function of dose from 0 up to 20 kGy.

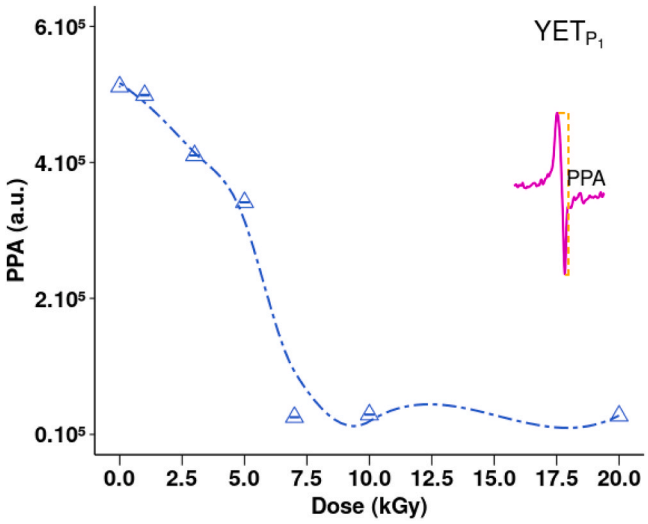

Fig. 6. Peak-peak amplitude (PPA) of the main EPR peak (P1) as a function of dose ranging from 0 up to 20 kGy.

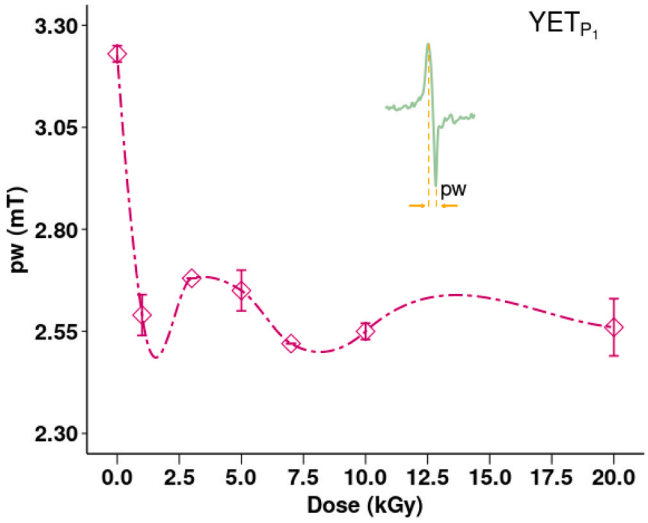

Fig. 7. Variation of peak-width (pw) of the main EPR peak (P_1) as a function of dose, ranging from 0 up to 20 kGy.

The EPR characterization of YET nanoparticles as synthesised and after exposed to ionizing radiation (^{60}Co) under a range of dose from 1 to 20 kGy provided important data on yttria electron defects, including the behaviour of its paramagnetic radicals e.g. g-value, PPA, and pw. The knowledge of how a material/substance response to ionizing radiation, which means a radiation dose, is a fundamental stage in the search process of new materials for radiation dosimetry.

4. Conclusion

Europium, thulium co-doped yttria (YET) powders, with cubic C-type form, mean particle size (d_{50}) 148 nm, and electron paramagnetic resonance (EPR) response as a function of dose, were successfully obtained by an alternative hydrothermal synthesis. YET nanoparticles prepared with 1.0 at%Tm presented an EPR spectra featured with a main peak (P_1) recorded at 335.52mT, g-value 2.0094, and peak width 3.23mT. Even if the peak-peak amplitude (P_1) of the powdered samples exhibited a decrement behaviour as a function of dose, it might be different using lower doses. These achievements are essential to go forward in the formation of new materials for radiation dosimetry.

Prime Novelty Statement

Yttria (Y_2O_3) also known as yttrium oxide is one of the most used rare-earth based oxides for advanced materials due to its special physical chemistry properties. Additionally, yttria properties can be improved by doping with others rare-earths elements (RE:Y_2O_3). However, most contributions from literature are limited to powders synthesis, while investigations on electronic defects induced by RE doping and ionizing radiation are very scarce.

The present paper innovates by evaluating the dose-response behaviour of europium, thulium co-doped yttria (YET) powders obtained by an alternative hydrothermal synthesis. YET nano-sized powders with narrow particle size distribution were formed using hydrothermal synthesis based on environmental pressure and temperature of 60°C. Besides, powder characteristics as particle size distribution, powder shape, crystalline structure, and electron density were investigated. Moreover, electron defects induced by dopant concentration and ionizing radiation (^{60}Co) were characterized by Electron Paramagnetic Resonance (EPR) under environmental temperature.

As exposed above, the paper is original, innovative and fits the scope of this journal. The achievements reported are useful parameters to advance toward formation of new materials for radiation dosimetry.

Consent for publication

We authors declare our consent for publication.

Ethics and consent to participate

No human or animal were used in the study

Funding

The authors would like to acknowledge the following sponsor organizations: São Paulo Research Foundation (FAPESP, grant# 2018/05982–0; grant#2022/06695–0), National Council for Scientific and Technological Development (CNPq, grant# 426513/2018–5), and Coordination for the Improvement of High Degree People (CAPES, grant#88882.315568/2019–01).

Declaration of Competing interest

The authors declare that they have no known competing financial interests or personal relationships that could have appeared to influence the work reported in this paper.

Acknowledments

We authors are deeply grateful to Dr. Maria Elisa Chuery Martins Rostelato from Radiation Technology Centre (CTR), Dr. Ivana Conte Cosentino from Science and Technology of Materials Centre (CCTM) both at Nuclear and Energy Research Institute (IPEN/CNEN-SP, Sao Paulo, Brazil). In addition our gratitude to the following sponsor organizations: São Paulo Research Foundation (FAPESP), grant#2022/06695–0; National Council for Scientific and Technological Development (CNPq); and Coordination for Improvement of High Degree People (CAPES).

This research used facilities of the Brazilian Nanotechnology National Laboratory (LNNano), part of the Brazilian Centre for Research in Energy and Materials (CNPEM), a private non-profit organization under the supervision of the Brazilian Ministry for Science, Technology, and Innovations (MCTI). The (Electron Microscopy) staff is acknowledged for the assistance during the experiments (SEM-FIB-C1–20222260).

Appendix A. : Chemical Composition of the rare-earth based starting materials used for synthesis of europium, thulium co-doped yttria (YET) nanoparticles

The chemical composition of the rare-earth based starting materials was characterized by Inductively Coupled Plasma Atomic Emission Spectrometry (ICP-AES, ICPE 9000, Shimadzu), and the results are presented in Tab.1, Tab.2, and Tab.3, respectively.

- Yttria (Y_2O_3)

Table 1
Main elements observed in the chemical composition of Y_2O_3 powders as received

Element	C (ppm)	Element	C (ppb)	Element	C (ppb)
Y	> 550	Th	510	Zr	43
Cs	65	Pr	260	Sc	15
Si	4,1	Mo	180	Eu	14
Rh	3,5	Ta	160	Ga	13
Ge	1,3	Na	130	Mg	3.3
Pt	1,1	Cr	100	Be	1.9
		Ca	49	Al	1.4

C: concentration; ppm: parts per million; ppb: parts per billion.

- Europium Oxide (Eu_2O_3)

Table 2
Main elements observed in the chemical composition of Eu_2O_3 powders as received

Element	C (ppm)	Element	C (ppb)	Element	C (ppb)
Eu	> 1000	Na	860	Gd	210
Cs	280	Sn	790	Nb	200
Rh	22	Ge	780	Sc	190
Si	4,4	Dy	710	Pb	190
Th	3,9	Bi	530	Ta	190
U	2,2	Sm	520	Tb	160

(*continued on next page*)

Table 2 (*continued*)

Element	C (ppm)	Element	C (ppb)	Element	C (ppb)
Cu	1,5	Ce	460	Er	150
P	1,5	Hf	460	Y	50
Pr	1,4	Tm	240	Al	1.1

C: concentration; ppm: parts per million; ppb: parts per billion.

- Thulium Oxide (Tm_2O_3)

Table 3
Main elements observed in the chemical composition of Tm_2O_3 powders as received

Element	C (ppm)	Element	C (ppb)	Element	C (ppb)
Tm	> 1000	Ta	870	Nb	410
Cs	800	Os	740	Ru	390
Rb	140	Ge	730	Er	360
Rh	52	Mo	630	Hf	270
Co	12	Na	500	Pb	270
Th	12	Sm	490	Fe	220
Ir	5.9	V	480	Zr	210
Si	4.3	Ho	440	Y	47
W	2.2	Ga	430	Al	1.8

C: concentration; ppm: parts per million; ppb: parts per billion.

Data availability

We cannot share any data today due to a hacker attack to our server. The data will be available as soon as this issue is solved.

References

[1] V. Chopra, Y.R. Parauha, D. Poelman, S.J. Dhoble, Principle, mechanism, and models of radiation dosimetry, in: S. Dhoble, V. Chopra, V. Nayar, G. Kitis, D. Poelman, H.B.T.-R.D.P. Swart (Eds.), Woodhead Publishing Series in Electronic and Optical Materials, Woodhead Publishing, 2022, pp. 27–45, https://doi.org/10.1016/B978-0-323-85471-9.00012-9.

[2] N. Kataoka, D. Kawahara, M. Sekiguchi, Uniform irradiation of table eggs in the shell with low-energy electron beams, Radiat. Phys. Chem. 202 (2023) 110553, https://doi.org/10.1016/j.radphyschem.2022.110553.

[3] O. Turan, A.O. Cetintas, M. Gokalp, H.B. Halkman, E. Ic, O. Kantoglu, K. Y. Kantoglu, Assessment of Low-Energy electron beam irradiation for effective surface microbial decontamination of fresh lettuce (Lactuca sativa L.) leaves, Food Control (2025) 111423, https://doi.org/10.1016/j.foodcont.2025.111423.

[4] A.A. Chowdhury, S. Bolton, G. Lowe, E. Vasquez Osorio, W. Hamblyn, P.J. Hoskin, The clinical application of in vivo dosimetry for gynaecological brachytherapy: a scoping review, Tech. Innov. Patient Support Radiat. Oncol. 33 (2025) 100290, https://doi.org/10.1016/j.tipsro.2024.100290.

[5] J.A.C. Gonçalves, V.K. Asfora, H.J. Khoury, C.C. Bueno, Characterization of a 1.5 MeV electron beam irradiator using a homemade diode-based dosimetry system, Radiat. Phys. Chem. (2025) 112880, https://doi.org/10.1016/j.radphyschem.2025.112880.

[6] P. Cheilas, T. Christou, S. Karkalakos, C. Kottaridi, P.G. Michaelides, Rare earth elements and the US renewable economy: a causality exploration between critical materials and clean energy, Resour. Policy 101 (2025) 105491, https://doi.org/10.1016/j.resourpol.2025.105491.

[7] V. Rizos, E. Righetti, A. Kassab, Understanding the barriers to recycling critical raw materials for the energy transition: the case of rare earth permanent magnets, Energy Rep. 12 (2024) 1673–1682, https://doi.org/10.1016/j.egyr.2024.07.022.

[8] D. Brown, R. Zhou, M. Sadan, Critical minerals and rare earth elements in a planetary just transition: an interdisciplinary perspective, Extr. Ind. Soc. 19 (2024) 101510, https://doi.org/10.1016/j.exis.2024.101510.

[9] L. Depraiter, S. Goutte, Geopolitical risk and clean energy investments: exploring the role of rare earths, Int. Rev. Financ. Anal. 100 (2025) 103965, https://doi.org/10.1016/j.irfa.2025.103965.

[10] S.C. Gedam, S. Dhoble, Effect of gamma-radiation on NaZnSO4Cl:Ce, dy or mn ions and retrapping of charges in TL, J. Lumin. 142 (2013) 139–143.

[11] T.N. Megharaj, B.R.R. Krushna, I.S. Pruthviraj, S.C. Sharma, K. Manjunatha, S. Y. Wu, R. Arunakumar, F.F. Komahal, G. Ramakrishna, H. Nagabhushana, Luminescence and structural insights of β-Ca2SiO4:Pr3+ phosphor: applications towards TL dosimetry and solid state lighting, Mater. Chem. Phys. 334 (2025) 130508, https://doi.org/10.1016/j.matchemphys.2025.130508.

[12] S. Kadam, S.N. Menon, P. Rama, R. Yadav, S. Dawn, B. Dhabekar, Beta dose rate estimation of soil samples with CW-OSL technique using LiCaAlF6:Eu,Y phosphor for retrospective dosimetry, Radiat. Phys. Chem. 223 (2024) 111968, https://doi.org/10.1016/j.radphyschem.2024.111968.

[13] K. Zhang, T. Li, X. Liu, Z. Huang, Y. Liu, The formation process and influencing factors of electric field-induced oxygen vacancy in Y2O3 transparent ceramic, Ceram. Int. 50 (2024) 41417–41425, https://doi.org/10.1016/j.ceramint.2024.07.456.

[14] S.G. Nath, A. E I, A critical review focussing on the synthesis and applications of monoclinic yttrium oxide nanophosphor, Mater. Res. Bull. 182 (2025) 113128, https://doi.org/10.1016/j.materresbull.2024.113128.

[15] S.A.M. Issa, D.E. Abulyazied, A.W. Alrowaily, H.A. Saudi, E.S. Ali, A.M.A. Henaish, H.M.H. Zakaly, Improving electrical, optical and radiation shielding properties of polyvinyl alcohol yttrium oxide composites, J. Rare Earths 41 (2023) 2002–2009, https://doi.org/10.1016/j.jre.2023.02.013.

[16] B. Wang, Q. Jin, X. Du, C. Wang, G. Li, Y. Zheng, H. Sun, D. Zhang, C. Ma, Corrosion mechanism and microstructure evolution of yttrium-doped marine steel, J. Mater. Res. Technol. 28 (2024) 2752–2766, https://doi.org/10.1016/j.jmrt.2023.12.189.

[17] P. Ren, X. Wang, M. Zhang, X. Sun, Fabrication of yttrium oxide refractory with high strength and thermal shock stability for smelting TiAl alloy, Ceram. Int. 50 (2024) 464–473, https://doi.org/10.1016/j.ceramint.2023.10.122.

[18] T.A. Nhlapo, S.T. Dlamini, T.P. Mokoena, T.C. Mokhena, T.S. Mahule, T.D. Malevu, T. Moyo, Influence of rare-earth elements (RE = Ce, Nd, Gd) on structural, ESR and Mössbauer spectroscopy studies of Ni0.5Co0.5RE0.03Fe1.97O4 synthesized by glycol-thermal method, J. Solid State Chem. 330 (2024) 124479, https://doi.org/10.1016/j.jssc.2023.124479.

[19] R.E. Riman, Powders, solution synthesis of, in: K.H.J. Buschow, R.W. Cahn, M. C. Flemings, B. Ilschner, E.J. Kramer, S. Mahajan, P. Veyssière (Eds.), Encyclopedia of Materials: Science and Technology, Elsevier, Oxford, 2001, pp. 7800–7811, https://doi.org/10.1016/B0-08-043152-6/01402-9.

[20] B. Panchal, O. Toikkanen, S. Hokkanen, M. Outinen, A. Heino, R. Partanen, Interactive role of particle size, shape, and structure in impact strength and breakage behavior of agglomerated dairy powders, Powder Technol. 452 (2025) 120595, https://doi.org/10.1016/j.powtec.2024.120595.

[21] S. Bau, S. Artous, S. Jacquinot, D. Locatelli, J.-F. Hochepied, N. Feltin, C. Chivas-Joly, Impact of the polydispersion of TiO2 materials on their particle size calculated from specific surface area results obtained during an interlaboratory comparison exercise, Particuology 98 (2025) 31–40, https://doi.org/10.1016/j.partic.2025.01.002.

[22] Y. Li, G. Buscarnera, Role of the particle size and shape dispersion on stress transmission and strain energy storage, Geotech. Lett. 15 (2025) 45–51, https://doi.org/10.1680/jgele.24.00056.

[23] W. Jin, D. Huo, J. Gao, C. E, Y. Fan, C. Lu, Mixing and flow characteristics of binary particles with a significant difference in particle size in a coupled fluidized bed, Chem. Eng. J. 509 (2025) 161294, https://doi.org/10.1016/j.cej.2025.161294.

[24] K. Kitamura, T. Mori, Effect of particle concentration during kneading on the particle dispersion state of carbon slurry, Chem. Eng. Sci. 302 (2025) 120897, https://doi.org/10.1016/j.ces.2024.120897.

[25] J. Li, Y. Qin, J. Zhang, A. Zhang, X. Zhang, Compaction and shear characteristics of recycled construction & demolition aggregates in subgrade: exploring particle breakage and shape effects, J. Clean. Prod. 465 (2024) 142776, https://doi.org/10.1016/j.jclepro.2024.142776.

[26] F. Liu, Q. Xu, J. Qu, Y. Huang, J. Ma, L. Lin, Effect of silica particle size on the viscosity, curing behavior, and sintering performance of silica/alumina ceramic suspensions for digital light processing-based vat photopolymerization, Ceram. Int. (2025), https://doi.org/10.1016/j.ceramint.2025.03.036.

[27] M. Momtaz, J.L. McNanna, M. Schoenitz, E.L. Dreizin, Effect of powder characteristics on thermal oxidation of boron, Thermochim. Acta 743 (2025) 179917, https://doi.org/10.1016/j.tca.2024.179917.

[28] S.C. Santos, C. Yamagata, A.C. Silva, L.F.G. Setz, S.R.H. Mello-Castanho, Yttrium disilicate micro-cellular architecture from biotemplating of luffa cylindrica,

J. Ceram. Sci. Technol. 5 (2014) 203–208, https://doi.org/10.4416/JCST2014-00008.
[29] S.C. Santos, C. Yamagata, L.L. Campos, S.R.H. Mello-Castanho, Processing and thermoluminescent response of porous biomorphic dysprosium doped yttrium disilicate burner, Mater. Chem. Phys. 177 (2016) 505–511, https://doi.org/10.1016/j.matchemphys.2016.04.061.
[30] S.C. Santos, O. Rodrigues, L.L. Campos, Bio-prototyping of europium-yttria based rods for radiation dosimetry, Mater. Chem. Phys. (2017), https://doi.org/10.1016/j.matchemphys.2017.07.063.
[31] S.C. Santos, O. Rodrigues Jr, L.L. Campos, Effect of thulium on promotion of dose-response behaviour of yttria based rods by electron paramagnetic resonance, J. Alloy. Compd. 1003 (2024) 175583, https://doi.org/10.1016/j.jallcom.2024.175583.
[32] S.C. Santos, O. Rodrigues, L.L. Campos, Building up europium thulium co-doped yttria nanoparticles with electron paramagnetic resonance response by colloidal synthesis, Materialia 30 (2023) 101829, https://doi.org/10.1016/j.mtla.2023.101829.
[33] N. Doebelin, R. Kleeberg, Profex: a graphical user interface for the rietveld refinement program, J. Appl. Crystallogr. 48 (2015) 1573–1580, https://doi.org/10.1107/S1600576715014685.
[34] K. Momma, F. Izumi, VESTA: a three-dimensional visualization of crystal, volumetric and morphology data, J. Appl. Crystallogr. 44 (2011) 1272–1276, https://doi.org/10.1107/S0021889811038970.
[35] J.P. Coutures, R. Verges, M. Foex, Comparison of solidification temperatures of different rare earth sesquioxides; effect of atmosphere, Rev. Int. Des. Hautes Temp. Et. Des. Refract. 12 (1975) 181–185.
[36] W. Tscharnuter, Photon Correlation Spectroscopy in Particle Sizing, John Wiley & Sons Ltd, United States of America, 2000. ⟨http://www.brookhaveninstruments.com/literature/lit_90Plus.html⟩.
[37] L. Kovarik, M. Bowden, J. Szanyi, High temperature transition aluminas in δ-Al2O3/θ-Al2O3 stability range: review, J. Catal. 393 (2021) 357–368, https://doi.org/10.1016/j.jcat.2020.10.009.
[38] R. Rothon, P. Hornsby, Chapter 9 - fire retardant fillers for polymers, in: C. D. Papaspyrides, P. Kiliaris (Eds.), Polymer Green Flame Retardants, Elsevier, Amsterdam, 2014, pp. 289–321, https://doi.org/10.1016/B978-0-444-53808-6.00009-3.
[39] M. Kumar, J. Dutta Majumdar, I. Manna, Development of Gd2O3 doped yttria stabilized zirconia based thermal barrier coating for improved high temperature oxidation and erosion resistance, Ceram. Int. 49 (2023) 38081–38093, https://doi.org/10.1016/j.ceramint.2023.09.138.
[40] N. Putenpurayil Govindan, A. Najafzadehkhoee, A. Talimian, V. Pouchly, M. Michálková, P. Švančárek, R. Klement, D. Galusek, Sintering of Ce3+-doped yttria nanoparticles prepared by precipitation method, Open Ceram. 13 (2023) 100315, https://doi.org/10.1016/j.oceram.2022.100315.
[41] S. Li, S. Xu, X. Wang, D. Wang, B.A. Goodman, X. Hong, W. Deng, Optical properties of gadolinia-doped cubic yttria stabilized zirconia single crystals, Ceram. Int. 47 (2021) 3346–3353, https://doi.org/10.1016/j.ceramint.2020.09.178.
[42] J. Li, L. Fan, N. Hou, Y. Zhao, Y. Li, Solid oxide fuel cell with a spin-coated yttria stabilized zirconia/gadolinia doped ceria bi-layer electrolyte, RSC Adv. 12 (2022) 13220–13227, https://doi.org/10.1039/d2ra02035a.
[43] N.J. Shivaramu, B.N. Lakshminarasappa, K.R. Nagabhushana, F. Singh, E. Coetsee, H.C. Swart, Photoluminescence and thermoluminescence studies of 100 MeV Si8+ ion irradiated Y2O3:Dy3+ nanophosphor, J. Lumin. 209 (2019) 179–187, https://doi.org/10.1016/j.jlumin.2019.01.049.
[44] S.C. Santos, O. Rodrigues, L.L. Campos, EPR response of yttria micro rods, J. Alloy. Compd. (2018), https://doi.org/10.1016/j.jallcom.2018.06.063.
[45] S.C. Santos, O. Rodrigues, L.L. Campos, EPR dosimetry of yttria micro rods, J. Alloy. Compd. (2018), https://doi.org/10.1016/j.jallcom.2018.01.315.
[46] S.C. Santos, O. Rodrigues Jr, L.L. Campos, Effect of thulium on promotion of dose-response behaviour of yttria based rods by electron paramagnetic resonance, J. Alloy. Compd. 1003 (2024) 175583, https://doi.org/10.1016/j.jallcom.2024.175583.
[47] J. Ren, J.X. Wu, P.P. Liu, Controlling the electronic and magnetic properties of ZnO monolayer by rare-earth atoms substitutional doping, Physica B Condensed Matter 652 (2023) 414661, https://doi.org/10.1016/j.physb.2023.414661.
[48] C. Li, H. Wei, Z. Li, X. Wang, The influence of rare earth (La, Ce, and Y) doping on the antibacterial properties of silver ions, Physica B Condensed Matter 675 (2024) 415648, https://doi.org/10.1016/j.physb.2023.415648.
[49] C.E. Secu, C. Bartha, C. Radu, M. Secu, Crystallization processes of rare-earth doped GdF3 nanocrystals in silicate glass matrix: dimorphism and photoluminescence properties, Ceram. Int. (2024), https://doi.org/10.1016/j.ceramint.2024.06.335.
[50] Z. Liao, Z. Yuan, H. Gao, F. Meng, Doped rare earth elements enhance gas sensing properties of hollow spiral-like Mn(OH)F semiconductor sensors for acetate esters detection, Sens. Actuators B Chem. 412 (2024) 135825, https://doi.org/10.1016/j.snb.2024.135825.
[51] D.B. Malavekar, V.V. Magdum, S.D. Khot, J.H. Kim, C.D. Lokhande, Doping of rare earth elements: towards enhancing the electrochemical performance of pseudocapacitive materials, J. Alloy. Compd. 960 (2023) 170601, https://doi.org/10.1016/j.jallcom.2023.170601.
[52] K. Riener, N. Albrecht, S. Ziegelmeier, R. Ramakrishnan, L. Haferkamp, A. B. Spierings, G.J. Leichtfried, Influence of particle size distribution and morphology on the properties of the powder feedstock as well as of AlSi10Mg parts produced by laser powder bed fusion (LPBF), Addit. Manuf. 34 (2020) 101286, https://doi.org/10.1016/j.addma.2020.101286.
[53] X. Qin, Y. Ju, S. Bernhard, N. Yao, Flame synthesis of y 2 o 3:Eu nanophosphors using ethanol as precursor solvents, J. Mater. Res. 20 (2005) 2960–2968, https://doi.org/10.1557/JMR.2005.0364.
[54] H. Starr, Territory, proximity, and spatiality: the geography of international conflict, Int. Stud. Rev. 7 (2005) 387–406, https://doi.org/10.1111/j.1551-2916.2005.00506.x.
[55] M.F. Rodrigues Pais Alves, C. Santos, S.M. Olhero, M.H.F. Vaz Fernandes, Pressureless sintered lithium disilicate glass-ceramics: influence of particle size and crystallization state, J. Eur. Ceram. Soc. 44 (2024) 6135–6146, https://doi.org/10.1016/j.jeurceramsoc.2024.03.012.
[56] C. Zhang, N. Zhang, J. Zhang, Y. Zhang, S. Cui, Y. Zhang, Surface modification of cast iron slag with rare earth coupling agent enhances mechanical and thermal properties of nonwoven geotextile trimmings-based composite plate, Surf. Interfaces 50 (2024) 104489, https://doi.org/10.1016/j.surfin.2024.104489.
[57] X. Yu, J. Ren, K. Gu, Q. Zhu, H. Cai, L. Zheng, W. Qiu, G. Chao, S. Gong, Synergistic improvement of mechanical properties and electrical conductivity of Cu-Fe alloys by rare earth metals sc and y addition, J. Alloy. Compd. 979 (2024) 173569, https://doi.org/10.1016/j.jallcom.2024.173569.
[58] Y. Zhu, Y. Deng, Y. An, K. Wang, R. Liu, L. Liu, Z. Wang, Y. Xiao, B. Wang, Effect of microalloying with rare-earth lanthanum on dynamic recrystallization behavior and mechanical properties of ti sheets, Mater. Today Commun. 39 (2024) 109155, https://doi.org/10.1016/j.mtcomm.2024.109155.
[59] X. Xiao, T. Tang, Q. Zhou, S. Li, J. Lv, M. Lou, K. Xu, L. Wang, K. Chang, Effects of rare earth oxide additions on the corrosion resistance of TiC-based cermets, Ceram. Int. 50 (2024) 12287–12297, https://doi.org/10.1016/j.ceramint.2024.01.133.
[60] F. Lu, X. Wang, Y. Ge, X. Sun, T. Zhao, X. Lu, Q. Fan, Nd3+-sensitized multilayered rare-earth nanocrystals with enhanced NIR-IIb luminescence for high resolution optical imaging, Ceram. Int. 50 (2024) 25060–25067, https://doi.org/10.1016/j.ceramint.2024.04.233.
[61] S.M. ul Hassan, W. Akram, A. Noureen, F. Ahmed, A. Hassan, A. Ullah, Advances in transition metals and rare earth elements doped ZnO as thermoluminescence dosimetry material, Radiat. Phys. Chem. 223 (2024) 111929, https://doi.org/10.1016/j.radphyschem.2024.111929.
[62] P. Dubey, J. Yogi, S. Kumar, S. Khatoon, K. Kumari, A. Anand, Shape-dependent size polydispersity: DEM investigation of mixing behavior in a vibrating packed bed system, Powder Technol. 441 (2024) 119804, https://doi.org/10.1016/j.powtec.2024.119804.
[63] X. Duan, Q. Liu, R. Zhao, W. Liu, L. Zhang, H. Hu, Effects of particle properties, intermolecular forces, and molecular structure on the shear-thickening behavior of waxy starch dispersions, Carbohydr. Polym. 334 (2024) 122004, https://doi.org/10.1016/j.carbpol.2024.122004.
[64] S. Roy, H. Xiao, V. Angelidakis, T. Pöschel, Combined thermal and particle shape effects on powder spreading in additive manufacturing via discrete element simulations, Powder Technol. (2024) 120099, https://doi.org/10.1016/j.powtec.2024.120099.
[65] Y. Wang, J. Xu, S. He, S. Liu, Z. Zhou, Effect of nuclei particle shape and baffle setting on the drum granulation in iron ore sintering process, Powder Technol. 433 (2024) 119222, https://doi.org/10.1016/j.powtec.2023.119222.
[66] Y. Li, Z. Guan, J. Jiang, L. Zhen, Evolution of the microstructure and electromagnetic properties of Fe–Si–Al particles during post ball-milling annealing, J. Mater. Res. Technol. 29 (2024) 3532–3542, https://doi.org/10.1016/j.jmrt.2024.02.038.
[67] H. Jain, G. Gupta, D.P. Mondal, A.K. Srivastava, A. Pandey, S. k Srivastava, R. Kumar, Effect of particle shape on microstructure and compressive response of 316L SS foam by space holder technique, Mater. Chem. Phys. 271 (2021) 124924, https://doi.org/10.1016/j.matchemphys.2021.124924.
[68] S.I. Gad, M.A. Attia, M.A. Hassan, A.G. El-Shafei, A random microstructure-based model to study the effect of the shape of reinforcement particles on the damage of elastoplastic particulate metal matrix composites, Ceram. Int. 47 (2021) 3444–3461, https://doi.org/10.1016/j.ceramint.2020.09.189.
[69] K.P.K. Ajjarapu, S. Barui, K. Sudan, S. Khanjar, K. Kate, Ceramic fused filament fabrication (CF3) of alumina: influence of powder particle morphology on processing and microstructure, Open Ceram. 19 (2024) 100631, https://doi.org/10.1016/j.oceram.2024.100631.
[70] G. Liang, W. Yao, A. She, Rheology and microstructure of lithium slag/metakaolin geopolymer pastes: insights from particle packing and water dynamic evolution, J. Build. Eng. 95 (2024) 110261, https://doi.org/10.1016/j.jobe.2024.110261.
[71] Y. Dong, A. Chen, T. Yang, S. Gao, S. Liu, B. Guo, H. Jiang, Y. Shi, C. Yan, Microstructure evolution and mechanical properties of Al2O3 foams via laser powder bed fusion from al particles, Adv. Powder Mater. 2 (2023) 100135, https://doi.org/10.1016/j.apmate.2023.100135.
[72] A. Dupont, A. Largeteau, C. Parent, B. Le Garrec, J.M. Heintz, Influence of the yttria powder morphology on its densification ability, J. Eur. Ceram. Soc. 25 (2005) 2097–2103, https://doi.org/10.1016/j.jeurceramsoc.2005.03.016.
[73] T. Kinoshita, H. Hosono, Materials design and example of long lasting phosphorescent glasses utilizing electron trapped centers, J. NonCryst. Solids 274 (2000) 257–263, https://doi.org/10.1016/S0022-3093(00)00217-9.
[74] A.I. Kuznetsov, O. Kameneva, N. Bityurin, L. Rozes, C. Sanchez, A. Kanaev, Laser-induced photopatterning of organic–inorganic TiO2-based hybrid materials with tunable interfacial electron transfer, Phys. Chem. Chem. Phys. 11 (2009) 1248–1257, https://doi.org/10.1039/B814494J.
[75] H. Yamamoto, T. Matsuzawa, Mechanism of long phosphorescence of SrAl2O4:Eu2+, Dy3+ and CaAl2O4:Eu2+, Nd3+, J. Lumin. 72–74 (1997) 287–289, https://doi.org/10.1016/S0022-2313(97)00012-4.

[76] T. Matsuzawa, Y. Aoki, N. Takeuchi, Y. Murayama, A new long phosphorescent phosphor with high brightness, SrAl2 O 4: Eu2 +, Dy3 +, J. Electrochem. Soc. 143 (1996) 2670, https://doi.org/10.1149/1.1837067.
[77] Y. Osada, S. Koike, T. Fukushima, S. Ogasawara, T. Shikada, T. Ikariya, Oxidative coupling of methane over Y2o3-Cao catalysts, Appl. Catal. 59 (1990) 59–74, https://doi.org/10.1016/S0166-9834(00)82187-9.
[78] E.E. Brown, U. Hommerich, A. Bluiett, C. Kucera, J. Ballato, S. Trivedik, Near-Infrared and upconversion luminescence in Er:Y2O3 ceramics under 1.5 mu m excitation, J. Am. Ceram. Soc. 97 (2014) 2105–2110, https://doi.org/10.1111/Jace.12898.
[79] K. Zhang, T. Li, X. Liu, Z. Huang, Y. Liu, The formation process and influencing factors of electric field-induced oxygen vacancy in Y2O3 transparent ceramic, Ceram. Int. 50 (2024) 41417–41425, https://doi.org/10.1016/j.ceramint.2024.07.456.
[80] S.C. Santos, O. Rodrigues, L.L. Campos, EPR response of yttria micro rods activated by europium, J. Alloy. Compd. (2018), https://doi.org/10.1016/j.jallcom.2018.06.063.
[81] T. Mitsuma, Narrowing of resonance line by spin-lattice relaxation in the system K3 (Cr-Fe-Co) (CN)6, J. Phys. Soc. Jpn. 17 (1962) 128–135, https://doi.org/10.1143/JPSJ.17.128.